Engineering of the resistive switching properties in V_2O_5 thin film by atomic structural transition: Experiment and theory

Zhenni Wan,[1,a)] Hashem Mohammad,[1] Yunqi Zhao,[1] Cong Yu,[2] Robert B. Darling,[1] and M. P. Anantram[1]
[1]*Department of Electrical Engineering, University of Washington, Seattle, Washington 98105, USA*
[2]*Department of Electronic and Information Engineering, Beihang University, Beijing 100191, China*

(Received 25 June 2018; accepted 20 August 2018; published online 10 September 2018)

Bipolar resistive switching has been reported in ITO/V_2O_5/ITO structures. Synthesized from the sol-gel process, the nanostructured $V_2O_5{\cdot}nH_2O$ xerogel thin film endures significant structural transition during the post-annealing step. The impact of the structural transition of the V_2O_5 film on the resistive switching properties is studied in this work. The switching voltage decreases from 6.5 V to 3.0 V when the annealing temperature increases from 220 °C to 280 °C and then increases up to 5.0 V at 350 °C. Above the annealing temperature of 350 °C, the reversible switching characteristics disappear. The thermogravimetric measurement shows that intercalated H_2O molecules fully evaporate above 350 °C. X-ray diffraction shows that the xerogel phase gradually vanishes as the annealing temperature increases, and only α-V_2O_5 and β-V_2O_5 exist at high annealing temperatures. *Ab initio* simulations are performed to evaluate the formation energies of the oxygen vacancy in xerogel, α-V_2O_5, and β-V_2O_5 phases. The results are in good agreement with the experiments: the formation energy of the oxygen vacancy is significantly lower in xerogel than in α-V_2O_5 and β-V_2O_5, enabling the occurrence of reversible switching when the xerogel phase exists in the sandwich structure. *Published by AIP Publishing*. https://doi.org/10.1063/1.5045826

I. INTRODUCTION

Resistive random access memory (RRAM) is considered to be one of the most promising candidates for the next generation memory due to its high speed,[1,2] low power consumption,[1] and superior scalability.[2,3] Most RRAMs are based on Metal-Insulator-Metal (MIM) systems and employ transition metal oxides such as HfO_2,[1] TiO_2,[2] ZnO,[4] and ZrO_2[5] as the sandwiched insulator layer. A widely accepted mechanism for bipolar resistive switching, which means that SET and RESET operations require opposite voltage polarities, is the formation of conductive filaments consisting of oxygen vacancies in the oxide layers due to the applied electric field.[6–11] Reports have indicated that the crystallinity of the insulator layer plays an important role in determining the resistive switching performance[12] as the oxygen vacancy formation energies differ for amorphous and crystalline oxides. This fact provides insights into engineering the electrical switching properties for other oxygen vacancy based RRAMs.

Vanadium pentoxide (V_2O_5) is widely used as a cathode material for lithium batteries[13–15] due to its layered atomic structure[16,17] and the capability of storing intercalating ions.[18] ITO (indium tin oxide) is a heavily doped n-type semiconductor with a large bandgap of 4 eV.[19] Previously, a novel forming-free bipolar resistive memory was discovered in ITO/V_2O_5/ITO structures.[20] ITO coated glass with a sheet resistance of 10 Ω/sq is used as the substrate and bottom contact. A thin film of V_2O_5 consisting of overlapped nanoribbons with a thickness of 800 nm is deposited using the sol-gel process. A gentle pre-annealing at 220 °C is added for 1 h to reduce the amount of intercalated water molecules and prevent bubbling during the post-annealing process. The top layer of ITO (160 nm) is deposited by magnetron sputtering, and the measured sheet resistance is 50 Ω/sq. It was proposed that oxygen vacancies were formed in V_2O_5 at the top ITO/V_2O_5 interface due to the applied electric field and this creates a thin Schottky tunneling barrier which increases the overall resistance. The oxygen ions migrate into or out of the top ITO layer which consists of sufficient vacancies to achieve reversible switching. The formation of oxygen vacancies in the V_2O_5 layer is critical in the electrical switching process and can have a significant impact on the switching voltage, which is of great importance in terms of energy consumption and electrical stress to peripheral circuit elements. As the V_2O_5 film is synthesized from the sol-gel process, it will endure a drastic structural transition at various temperatures. In this work, we investigate the impact of the structural transition of the V_2O_5 thin film in the ITO/V_2O_5/ITO sandwich structure due to the post-annealing process at various temperatures. A significant change in resistive switching properties is found, and the underlying mechanism is attributed to the change in the oxygen vacancy formation energies resulting from phase transition from xerogel to α-/β-V_2O_5 when annealing temperature increases.

II. RESULTS

A. I-V Characteristics at various post-annealing temperatures

Current-voltage characteristics of ITO/V_2O_5/ITO devices are measured using a Keithley 4200SCS parameter

a)Author to whom correspondence should be addressed: jennywan@uw.edu.

analyzer after annealing at temperatures varying from 220 °C to 400 °C. The results are shown in Fig. 1.

Most of the devices show reversible bipolar switching behavior. Under high positive bias, the device can be switched from a low resistance state (LRS) to a high resistance state (HRS) without the forming process. HRS can be reset to LRS with a sufficient negative bias. The switching voltages are shown to depend significantly on the annealing temperature. As the annealing temperature increases from 220 °C, the positive switching voltage (for HRS state) drops from 6.5 V and reaches its minimum value of 3 V at 280 °C. Negative switching voltage does not show a monotonic change and varies around −2.0 V. Making the annealing temperature larger than 280 °C results in an increase in the magnitude of both the positive and negative switching voltages. When the annealing temperature is above 360 °C, the reversible resistive switching behavior disappears. Irreversible breakdown that causes the current to drop down to almost zero occurs when the positive or negative bias reaches about 4 V in magnitude. The results indicate that the switching behavior is optimized at an annealing temperature of 280 °C and is very sensitive to annealing temperatures above 320 °C.

The shape of I-V curves also changes significantly. At low annealing temperatures, resistance of the device is high at low biases and gradually decreases when the applied voltage increases, showing non-linear I-V characteristics. As the annealing temperature increases, this non-linear feature disappears, and the device exhibits Ohmic behavior for both LRS and HRS. The transition in low-bias I-V characteristics also indicates a change in the band structure in the transport direction. The underlying mechanism for the change in electrical properties is attributed to the change in the chemical composition and atomic structure of the $V_2O_5{\cdot}nH_2O$ thin film during the post-annealing process, which will be discussed in Secs. II B and III A.

B. TGA and x-ray diffraction analysis

A $V_2O_5{\cdot}nH_2O$ xerogel thin film synthesized by the sol-gel process contains intercalated H_2O molecules[16] which can be gradually evaporated when annealed. First, we evaluate the water content in $V_2O_5{\cdot}nH_2O$ xerogel as a function of the annealing temperature. Thermogravimetric analysis (TGA) is performed on a thermal gravimetric analyzer in a N_2 atmosphere, and the temperature is swept from room temperature to 500 °C with a heating rate of 5 °C/min.

The obtained thermogravimetric trace is shown in Fig. 2. It reveals the existence of 1.8 mole of water per mole of oxide at room temperature, assuming that H_2O is the only volatile phase in the xerogel film. The water content decreases rapidly and is characterized by the weight loss until the trace enters a gradually decreasing region above 70 °C. The value of n decreases to 0.25 at 270 °C followed by a sharp peak in derivative weight, indicating the loss of more tightly bound water. At 300 °C, the n value decreases to 0.05, and beyond 350 °C, the weight loss is no longer observed, suggesting that all the bound water has been released. Comparing the TGA results with the I-V characteristics mentioned above, it is intuitive to relate the water content to the change in switching properties. Below the optimized annealing temperature of 280 °C, the amount of H_2O molecules intercalated is relatively high, potentially creating a small barrier between V_2O_5 atomic layers which blocks the electron transport under low biases. As the annealing temperature increases beyond 360 °C, the bound H_2O molecules fully evaporate, and this results in a more compact atomic structure solely consisting of crystalline V_2O_5. The

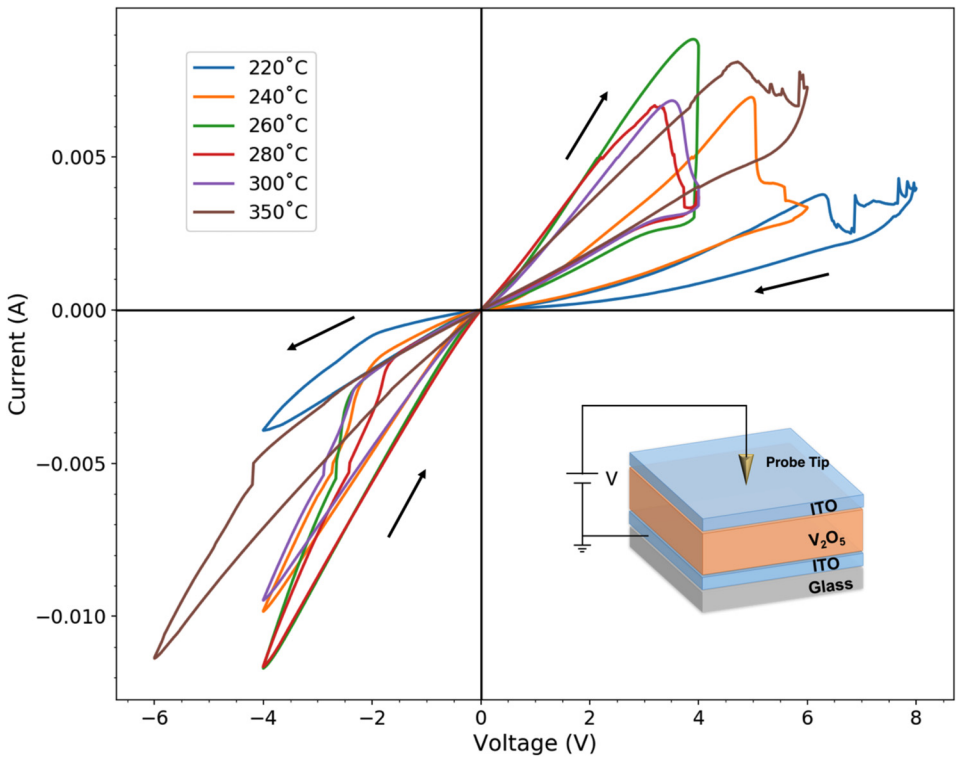


FIG. 1. I-V characteristics at various post-annealing temperatures from 220 °C to 350 °C. Minimum switching voltage is observed at 280 °C. (Inset) Structure of the ITO/V_2O_5/ITO device and bias setup.

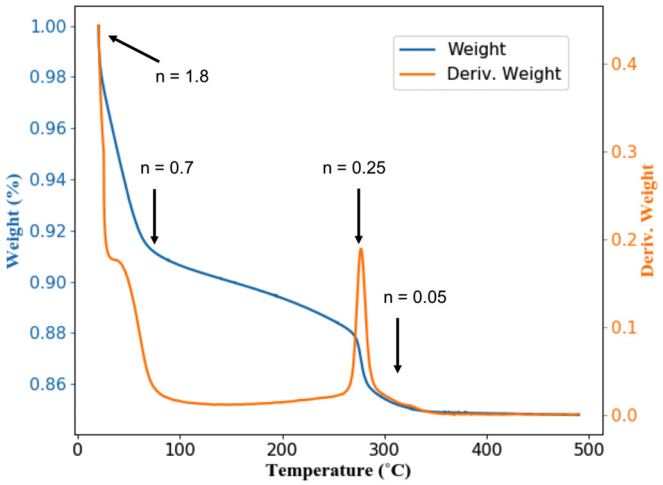


FIG. 2. Thermogravimetric analysis (TGA) of the V_2O_5 xerogel thin film and the corresponding calculated water content.

barrier for the generation of mobile ions is increased, resulting in the disappearance of reversible switching.

To further investigate the change in the atomic structure of the device, X-Ray Diffraction (XRD) analysis is performed on a Bruker F8 Focus Powder X-ray diffractometer using an X-ray source of Cu K-α radiation with a wavelength of 1.54 Å. The XRD patterns of the ITO/V_2O_5/ITO structure at various annealing temperatures are shown in Fig. 3. At low annealing temperatures below 280 °C, the dominant peak (001) is the one at 7.5°, indicating a large interlayer spacing of 11.78 Å with the presence of intercalated water molecules. The broad full-width at half-maximum (FWHM) of the dominant peak also indicates a large grain size, originated from the randomized overlapping of V_2O_5 nanoribbons during the sol-gel process. As the annealing temperature increases to 320 °C, the intensity of the low angle peak (7.5°) drops significantly and other minor peaks at around 10° begin to emerge. The dominant peak at 20.6° corresponds to a crystalline orthorhombic α-phase V_2O_5 (001)

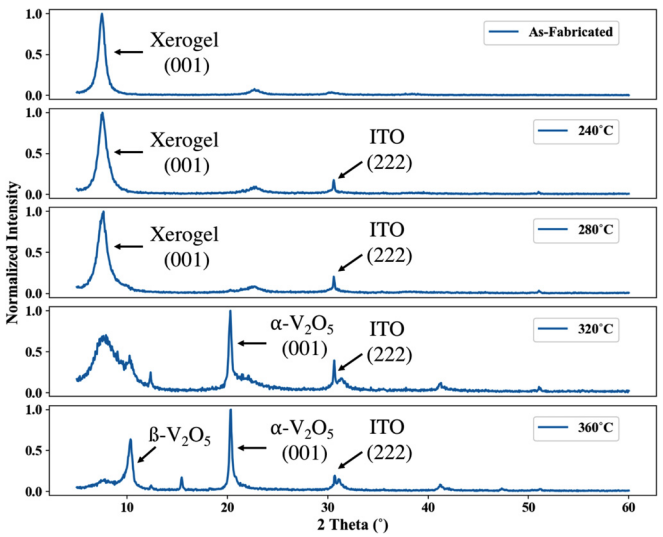


FIG. 3. XRD results of the ITO/V_2O_5/ITO structure at various annealing temperatures from the as-fabricated state to 360 °C. Distinct phase transition from the xerogel to α-/β-phase is observed above 320 °C.

peak. Interestingly, secondary peaks emerge at 11° and 12.5° as the annealing temperature becomes high, and they do not correspond to crystalline ITO or α-phase V_2O_5. These peaks belong to a different phase of V_2O_5, which is the β-phase. The existence of β-phase V_2O_5 in the ITO/V_2O_5/ITO structure is surprising, as previous reports have suggested that β-phase V_2O_5 is usually formed in rather extreme conditions: thermal heating of V_2O_5 powder at high temperature ($T = 1073$ K) and high pressure ($P = 6.0$ GPa)[21] or DC reactive magnetron sputtering at high substrate temperature ($T = 550$ °C).[22] In Sec. III A, it is discovered that the ultimate phase of the V_2O_5 film grown by the sol-gel process after high temperature annealing depends significantly on the properties of the substrate that the film is interfacing with.

III. DISCUSSIONS

A. Asymmetrical interfaces

To investigate the structural transition of the $V_2O_5{\cdot}nH_2O$ xerogel film during the annealing process and its dependence on the choice of the substrate material, the $V_2O_5{\cdot}nH_2O$ thin film was coated on three different substrates first: soda-lime microscope glass slide, sapphire, and ITO wafer. An ITO/V_2O_5/glass substrate structure was also fabricated to explore the effect of the top ITO film which was deposited by RF magnetron sputtering using the same recipe. The XRD analysis results of the four structures are shown in Fig. 4.

It is observed that at a high annealing temperature (400 °C), the crystal structure of the V_2O_5 film depends on the surface roughness of the substrate. When the substrate is crystalline and smooth (e.g., ITO or sapphire), the annealed V_2O_5 sol-gel film exhibits a regular α-phase with lattice constants of $a = 11.512$ Å, $b = 5.364$ Å, and $c = 4.368$ Å.[17] However, when the substrate is amorphous and rough (e.g., soda-lime glass has a roughness of ∼13 nm[23]), the crystal structure of the V_2O_5 film is in the β-phase and is identified by the dominant peak at 12.5° in the XRD analysis results.

The formation of the β-phase is explained by the different thermal expansion of the substrate and V_2O_5 film at the V_2O_5/substrate interface. Figure 5 shows the scanning electron microscopy (SEM) images of V_2O_5 nanoribbons synthesized by the sol-gel process from our previous work.[24] These nanoribbons are about 10 nm wide and 1 μm long and can easily fill into the valleys on a rough substrate. At high annealing temperatures, the nanoribbons that directly come into contact with the substrate can experience high localized pressure due to different thermal expansion coefficients (e.g., CTE is 9.5 ppm/K for soda-lime glass[25] and 51.6 ppm/K for V_2O_5[26]). The local high pressure provides the environment for the formation of β-phase V_2O_5 at the substrate/V_2O_5 interface, which acts as a seeding layer and eventually determines the crystal structure of the V_2O_5 film on the top. Whereas when the substrate surface is smooth, the overlap between the substrate and V_2O_5 nanoribbons is minimized and the local pressure does not reach the threshold for creating β-phase V_2O_5. Therefore, the film exhibits a normal crystal structure of α-phase V_2O_5. Note that in the ITO/V_2O_5/glass structure, the whole V_2O_5 film only exhibits a β-phase

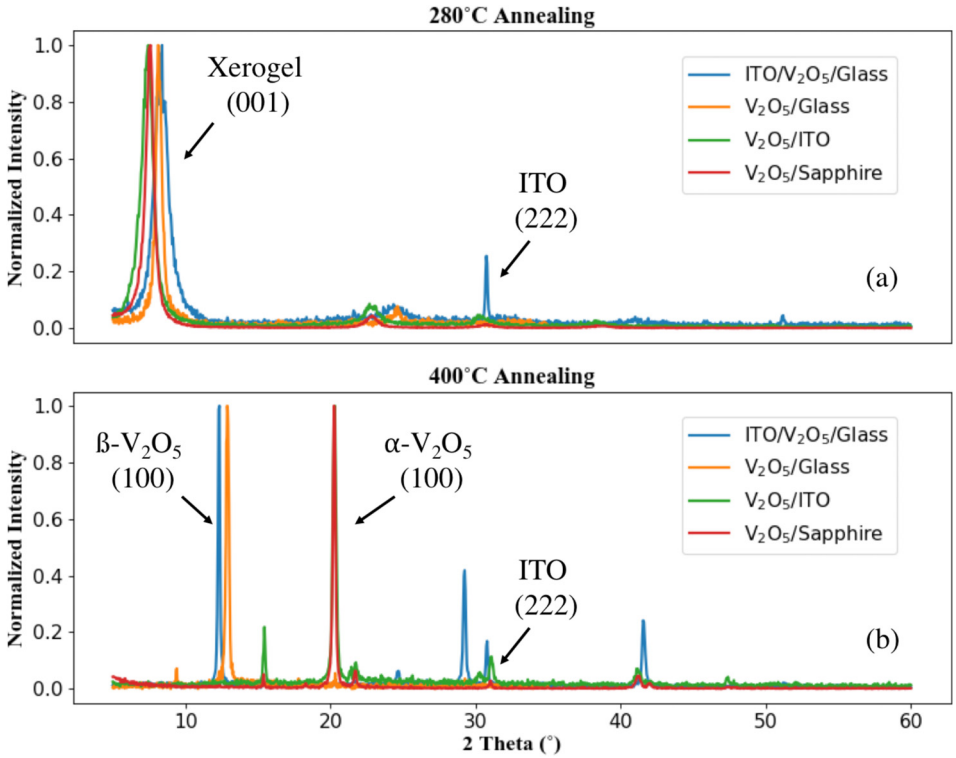


FIG. 4. XRD results of ITO/V_2O_5/Glass, V_2O_5/Glass, V_2O_5/ITO, and V_2O_5/Sapphire structures at annealing temperatures of (a) 280 °C and (b) 400 °C.

at 400 °C, in contrast to the α-V_2O_5 formed in the V_2O_5/ITO substrate structure. In this case, the V_2O_5 xerogel film becomes the rough substrate (surface roughness is around 30 nm[24]). During the subsequent magnetron sputtering deposition of top ITO, a firm interface with a large contact area is generated. β-phase V_2O_5 is thus formed at high annealing temperature due to the different thermal expansion of ITO and V_2O_5 (CTE is 7.2 ppm/K for ITO[27]).

From the above analysis, we conclude that the ITO/V_2O_5/ITO device has asymmetrical top and bottom interfaces. When the annealing temperature increases above 280 °C, α-V_2O_5 starts to form at the bottom ITO/V_2O_5 interface while β-V_2O_5 forms at the top ITO/V_2O_5 interface. The active region of the xerogel phase with large interlayer spacing is consumed and keeps shrinking. The phase distribution of the device is illustrated in Fig. 6(a). The resistive switching from LRS to HRS only occurs at positive bias, implying that the oxygen ion migration only happens between top ITO and V_2O_5 layers [Figs. 6(b) and 6(c)]. When β-V_2O_5 is formed at the top interface, it acts as a thin barrier layer for oxygen ion migration, where the xerogel region remains the source for mobile oxygen ions. This is consistent with the reduced ON/OFF ratio and increased switching voltages at annealing temperatures above 320 °C. At the same time, the α-V_2O_5 region at the bottom interface keeps growing and reduces the thickness of the xerogel region. At a high annealing temperature of 400 °C, the xerogel phase is thoroughly exhausted, accompanied by the disappearance of reversible resistive switching. This confirms that neither α-V_2O_5 nor β-V_2O_5 has the capability of generating oxygen ions and reacting with the ITO electrode to achieve reversible switching. To further investigate this claim, the results of first-principles calculations are presented in Sec. III B.

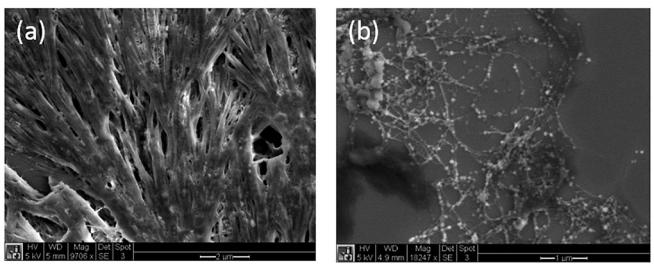


FIG. 5. SEM images of V_2O_5 nanoribbons on the silicon substrate (cited from Ref. 24).

B. Microscopic insights

We have confirmed that the presence of the xerogel phase is essential for creating oxygen vacancies in the V_2O_5 layer which is responsible for the resistive switching from LRS to HRS. First-principles calculations of oxygen vacancy formation energies in three different phases of V_2O_5 have been performed to obtain microscopic insights into our results. For all calculations, the spin polarized periodic DFT code Vienna *Ab-initio* Simulation Package[28,29] was employed, in which valence electronic states are described within a plane wave basis set with a cutoff energy of 520 eV. The core electrons were represented using projector augmented wave (PAW) pseudopotential[30] and explicitly treated eleven valence electrons for vanadium ($3p^6 3d^4 4s^1$), six for oxygen ($2s^2 2p^4$), and one for hydrogen. The Perdew-Burke-Ernzerhof[31] within the Generalized Gradient Approximation (GGA) functional[32] was used for the exchange-correlation energy, including rotationally invariant GGA+U[33] with a coulomb repulsion of U = 3.25 eV to account for the strongly correlated electrons in vanadium d-states.[34] Structural optimization was obtained by relaxing the atoms

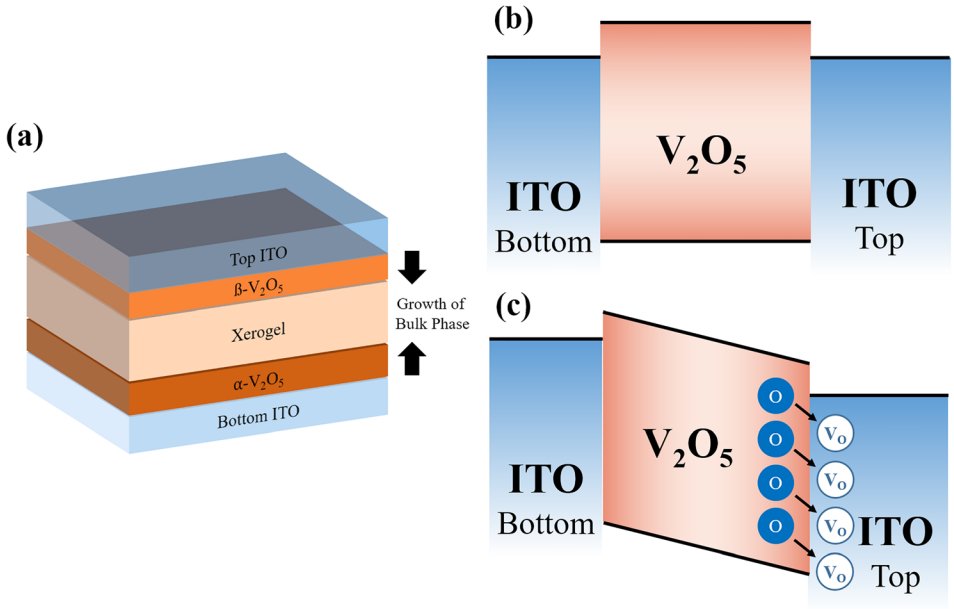


FIG. 6. (a) Phase distribution of the ITO/V_2O_5/ITO device at annealing temperature above 280 °C and below 400 °C. (b) Band diagram of the ITO/V_2O_5/ITO device without bias voltages. (c) Band diagram of the ITO/V_2O_5/ITO device with positive bias voltage. Oxygen ions migrate into vacancies in top ITO enhanced by the applied electric field.

using the conjugate-gradient method[35] with the use of a single gamma k-point.

Three different phases of V_2O_5 have been modeled to evaluate their oxygen vacancy formation energies, including α-phase, β-phase, and xerogel phase $V_2O_5{\cdot}0.5\ H_2O$. The value of n = 0.5 was chosen according to the TGA measurements at the optimized annealing temperature of 280 °C. The atomic structures denoted by distinct oxygen positions are shown in Fig. 7. Reduced V_2O_5 calculations were carried out on the $1 \times 4 \times 2$ supercell of $V_{32}O_{79}$ for α-V_2O_5 [Fig. 7(a)] and $2 \times 2 \times 3$ supercell of $V_{48}O_{119}$ for β-V_2O_5 [Fig. 7(b)]. $V_2O_5{\cdot}n\ H_2O$ xerogel consists of bilayer V_2O_5 layers intercalating H_2O molecules with an interlayer spacing of 10.49 Å. The $V_2O_5\ {\cdot}n\ H_2O$ xerogel structure has been explored experimentally and theoretically in previous works.[16,36–39] The structure of $V_2O_5{\cdot}0.5\ H_2O$ was obtained by first optimizing

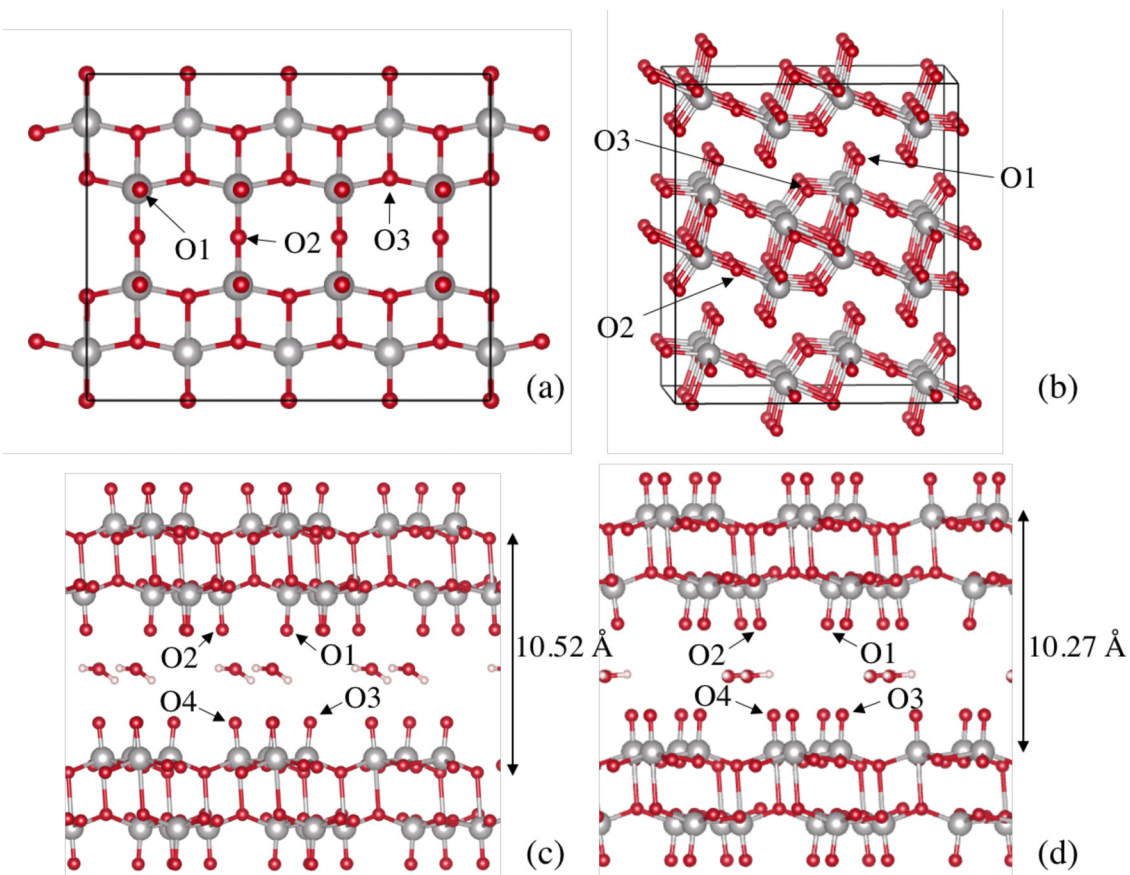


FIG. 7. Atomic structures of (a) α-V_2O_5, (b) β-V_2O_5, (c) $V_2O_5{\cdot}0.5\ H_2O$, type I, and (d) $V_2O_5{\cdot}0.5\ H_2O$ type II.

the $V_2O_5{\cdot}H_2O$ structure ($2 \times 4 \times 1$ supercell) reported in Ref. 37 and removing half of H_2O molecules followed by relaxing the structure again. As the water molecules in Ref. 37 have two different orientations, we have examined the cases of removing either type of water molecule [Figs. 7(c) and 7(d)]. An oxygen atom was then removed from the resulting structure for the oxygen vacancy formation energy calculations.

The energy of vacancy formation energy was calculated according to the following equation:

$$\Delta E^{V}_{form} = E^{V} - E^{prisine} + \frac{1}{2}\mu_{O_2},$$

where E^V is the energy of the system with a vacancy, $E^{prisine}$ is the energy of the system without the vacancy, and μ_{O_2} is the chemical potential of molecular oxygen.[40] In α-V_2O_5, only the O1 vacancy where the removed oxygen atom is bonded with a single vanadium atom has been taken into consideration as it has been reported to have the lowest formation energy.[41] The computed formation energy is 1.65 eV, and it is used as a reference to evaluate how easily the other structures could generate oxygen vacancies.

The calculated oxygen vacancy formation energies in β-V_2O_5 and two types of $V_2O_5{\cdot}0.5$ H_2O are listed in Table I. Note that in the xerogel structures, bridging oxygen sites that are bonded to multiple vanadium atoms are not considered as they are less likely to be removed from the system. The lowest formation energy found in β-V_2O_5 is 1.604 eV at the O1 site where the oxygen atom is bonded with a single vanadium atom. The difference in formation energy compared to α-V_2O_5 is only 46 meV, suggesting that both structures have a similar capability of generating oxygen vacancies. In the first type of $V_2O_5{\cdot}0.5$ H_2O, both O2 and O4 vacancy sites have lower formation energies than in the α-V_2O_5 case. In the second type of $V_2O_5{\cdot}0.5$ H_2O, the formation energies are further reduced and even become negative in the O4 vacancy site, implying that the release of oxygen atoms and generation of oxygen vacancies is a thermodynamically favored process. Taking a closer look at the resulting structure after removing the oxygen atom from the O4 site, it is found that one intercalated H_2O molecule has been attracted to the V_2O_5 laminar and filled the vacancy site [Fig. 8(b)]. Due to the heavy reconstruction occurring after the removal of the oxygen atom, the energy of the system decreased dramatically.

TABLE I. Energies of formation of oxygen vacancies in β-V_2O_5 and $V_2O_5{\cdot}0.5$ H_2O.

Vacancy site	Energy of formation (eV)	Difference from α-V_2O_5 (eV)
β-V_2O_5, O1 vacancy	1.604	−0.046
β-V_2O_5, O2 vacancy	2.543	0.893
β-V_2O_5, O3 vacancy	2.034	0.384
$V_2O_5{\cdot}0.5$ H_2O type I, O1	2.230	0.580
$V_2O_5{\cdot}0.5$ H_2O type I, O2	1.367	−0.283
$V_2O_5{\cdot}0.5$ H_2O type I, O3	2.205	0.555
$V_2O_5{\cdot}0.5$ H_2O type I, O4	1.302	−0.348
$V_2O_5{\cdot}0.5$ H_2O type II, O1	1.186	−0.464
$V_2O_5{\cdot}0.5$ H_2O type II, O2	0.957	−0.693
$V_2O_5{\cdot}0.5$ H_2O type II, O3	1.819	0.169
$V_2O_5{\cdot}0.5$ H_2O type II, O4	−0.628	−1.022

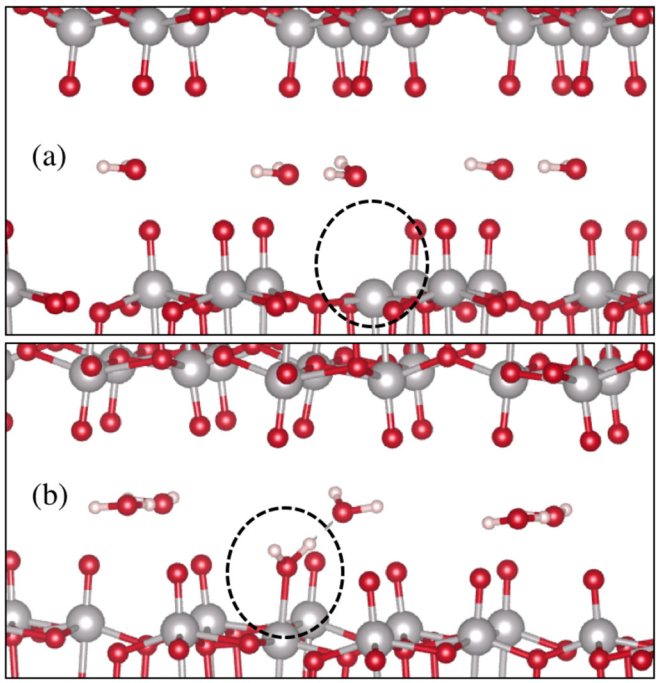


FIG. 8. Atomic structure after removing the oxygen atom and relaxation for (a) $V_2O_5{\cdot}0.5$ H_2O type II, O3 site and (b) $V_2O_5{\cdot}0.5$ H_2O type II, O4 site.

Our simulation results are in good agreement with the experiments and the physical models proposed for the switching mechanism. When intercalated H_2O molecules still exist in the V_2O_5 film, the interlayer spacing is enlarged so that the removal of single-bonded oxygen atoms becomes easier, resulting in a significant decrease in formation energies of the oxygen vacancy. The negative formation energy of the oxygen vacancy site (O4) in the type II xerogel structure also qualitatively agrees with the experimental observation that the color of fabricated device usually turned from orangish to greenish after a few weeks, indicating a spontaneous reduction of oxidation states. Above the annealing temperature of 360 °C, H_2O molecules have been fully removed from the V_2O_5 film so that only α-V_2O_5 and β-V_2O_5 exist. Reversible switching does not occur due to the relatively high formation energies of oxygen vacancies in these two compact crystalline phases.

IV. CONCLUSION

In this work, we investigate the effects of post-annealing temperatures on the switching characteristics of the ITO/V_2O_5/ITO device. At low annealing temperatures below 280 °C, intercalated water molecules increase the barrier for electron transport in the V_2O_5 xerogel film, thus resulting in non-linear I-V characteristics and higher switching voltages. When the annealing temperature is above 300 °C, phase transition starts to occur at both ITO/V_2O_5 interfaces: α-V_2O_5 is formed at the bottom and β-V_2O_5 is formed at the top, which gives a decreased ON/OFF ratio and higher switching voltages. The reversible resistive switching requires the

existence of the xerogel phase in the system. The annealing temperature is optimized at 280–300 °C. *Ab initio* simulations confirm that the formation energies of V_2O_5 xerogel are lower than those of both α-V_2O_5 and β-V_2O_5, in agreement with the experimental evidence that reversible resistive switching only occurs when the xerogel phase still exists in the V_2O_5 thin film.

[1]H. Lee, P. Che, T. Wu, Y. Che, C. Wan, P. Tzen, C. Lin, F. Chen, C. Lien, and M. Tsai, paper presented at the Electron Devices Meeting, 2008. IEDM 2008, IEEE International, 2008.
[2]Y. C. Yang, F. Pan, Q. Liu, M. Liu, and F. Zeng, Nano Lett. **9**(4), 1636–1643 (2009).
[3]B. Govoreanu, G. Kar, Y. Chen, V. Paraschiv, S. Kubicek, A. Fantini, I. Radu, L. Goux, S. Clima, and R. Degraeve, paper presented at the Electron Devices Meeting (IEDM), 2011, IEEE International, 2011.
[4]W.-Y. Chang, Y.-C. Lai, T.-B. Wu, S.-F. Wang, F. Chen, and M.-J. Tsai, Appl. Phys. Lett. **92**(2), 022110 (2008).
[5]C. Y. Lin, C. Y. Wu, C. Y. Wu, T. C. Lee, F. L. Yang, C. Hu, and T. Y. Tseng, IEEE Electron Device Lett. **28**(5), 366–368 (2007).
[6]J. J. Yang, M. D. Pickett, X. Li, D. A. Ohlberg, D. R. Stewart, and R. S. Williams, Nat. Nanotechnol. **3**(7), 429–433 (2008).
[7]N. Xu, L. Liu, X. Sun, X. Liu, D. Han, Y. Wang, R. Han, J. Kang, and B. Yu, Appl. Phys. Lett. **92**(23), 232112 (2008).
[8]M. Janousch, G. I. Meijer, U. Staub, B. Delley, S. F. Karg, and B. P. Andreasson, Adv. Mater. **19**(17), 2232–2235 (2007).
[9]G. Bersuker, D. C. Gilmer, D. Veksler, P. Kirsch, L. Vandelli, A. Padovani, K. M. L. Larcher, A. Shluger, V. Iglesias, M. Porti, and a. M. Nafría, J. Appl. Phys. **110**(12), 124518 (2011).
[10]D.-H. Kwon, K. M. Kim, J. H. Jang, J. M. Jeon, M. H. Lee, G. H. Kim, X.-S. Li, G.-S. Park, B. Lee, and S. Han, Nat. Nanotechnol. **5**(2), 148–153 (2010).
[11]S. Yu, X. Guan, and H.-S. P. Wong, Appl. Phys. Lett. **99**(6), 063507 (2011).
[12]P. Calka, M. Sowinska, T. Bertaud, D. Walczyk, J. Dabrowski, P. Zaumseil, C. Walczyk, A. Gloskovskii, X. Cartoixà, and J. Suñé, ACS Appl. Mater. Interfaces **6**(7), 5056–5060 (2014).
[13]S. H. Ng, S. Y. Chew, J. Wang, D. Wexler, Y. Tournayre, K. Konstantinov, and H. K. Liu, J. Power Sources **174**(2), 1032–1035 (2007).
[14]A. M. Cao, J. S. Hu, H. P. Liang, and L. J. Wan, Angew. Chem., Int. Ed. **44**(28), 4391–4395 (2005).
[15]J. Liu, H. Xia, D. Xue, and L. Lu, J. Am. Chem. Soc. **131**(34), 12086–12087 (2009).
[16]V. Petkov, P. N. Trikalitis, E. S. Bozin, S. J. L. Billinge, T. Vogt, and M. G. Kanatzidis, J. Am. Chem. Soc. **124**(34), 10157–10162 (2002).
[17]R. Enjalbert and J. Galy, Acta Crystallogr., Sect. C: Cryst. Struct. Commun. **42**(11), 1467–1469 (1986).
[18]Y. L. Cheah, V. Aravindan, and S. Madhavi, J. Electrochem. Soc. **159**(3), A273–A280 (2012).
[19]H. Kim and a. C. M. Gilmore, J. Appl. Phys. **86**(11), 6451–6461 (1999).
[20]Z. Wan, R. B. Darling, A. Majumdar, and M. P. Anantram, Appl. Phys. Lett. **111**(4), 041601 (2017).
[21]V. Filonenko, M. Sundberg, P.-E. Werner, and I. Zibrov, Acta Crystallogr., Sect. B: Struct. Sci. **60**(4), 375–381 (2004).
[22]Q. Su, W. Lan, Y. Wang, and X. Liu, Appl. Surf. Sci. **255**(7), 4177–4179 (2009).
[23]F. Roumili, S. Benbahouche, and J.-C. Sangleboeuf, Friction **3**(1), 65–71 (2015).
[24]Z. Wan, R. B. Darling, and M. Anantram, Phys. Chem. Chem. Phys. **17**(45), 30248–30254 (2015).
[25]T. P. Seward and T. Vascott, *High Temperature Glass Melt Property Database for Process Modeling* (Wiley, 2005).
[26]B. Singh, M. K. Gupta, S. K. Mishra, R. Mittal, P. U. Sastry, S. Rols, and S. L. Chaplot, Phys. Chem. Chem. Phys. **19**(27), 17967–17984 (2017).
[27]W.-F. Wu and B.-S. Chiou, Thin Solid Films **293**(1), 244–250 (1997).
[28]G. Kresse and J. Hafner, Phys. Rev. B **49**(20), 14251–14269 (1994).
[29]G. Kresse and J. Furthmüller, Phys. Rev. B **54**(16), 11169–11186 (1996).
[30]P. E. Blöchl, Phys. Rev. B **50**(24), 17953–17979 (1994).
[31]J. P. Perdew, K. Burke, and M. Ernzerhof, Phys. Rev. Lett. **77**(18), 3865–3868 (1996).
[32]J. P. Perdew, J. A. Chevary, S. H. Vosko, K. A. Jackson, M. R. Pederson, D. J. Singh, and C. Fiolhais, Phys. Rev. B **46**(11), 6671–6687 (1992).
[33]A. I. Liechtenstein, V. I. Anisimov, and J. Zaanen, Phys. Rev. B **52**(8), R5467–R5470 (1995).
[34]L. Wang, T. Maxisch, and G. Ceder, Phys. Rev. B **73**(19), 195107 (2006).
[35]W. H. Press, *Numerical Recipes: The Art of Scientific Computing* (Cambridge University Press, New York, 1986).
[36]H. H. Kristoffersen and H. Metiu, J. Phys. Chem. C **120**(7), 3986–3992 (2016).
[37]V. V. Porsev, A. V. Bandura, and R. A. Evarestov, Surf. Sci. **666**(Suppl. C), 76–83 (2017).
[38]G. Sai Gautam, P. Canepa, W. D. Richards, R. Malik, and G. Ceder, Nano Lett. **16**(4), 2426–2431 (2016).
[39]N. Sa, T. L. Kinnibrugh, H. Wang, G. Sai Gautam, K. W. Chapman, J. T. Vaughey, B. Key, T. T. Fister, J. W. Freeland, D. L. Proffit, P. J. Chupas, G. Ceder, J. G. Bareno, I. D. Bloom, and A. K. Burrell, Chem. Mater. **28**(9), 2962–2969 (2016).
[40]C. Freysoldt, B. Grabowski, T. Hickel, J. Neugebauer, G. Kresse, A. Janotti, and C. G. Van de Walle, Rev. Mod. Phys. **86**(1), 253–305 (2014).
[41]D. O. Scanlon, A. Walsh, B. J. Morgan, and G. W. Watson, J. Phys. Chem. C **112**(26), 9903–9911 (2008).